Life Sciences 237 (2019) 116902

Contents lists available at ScienceDirect

Life Sciences

journal homepage: www.elsevier.com/locate/lifescie

The lncRNA NEAT1/miR-29b/Atg9a axis regulates IGFBPrP1-induced autophagy and activation of mouse hepatic stellate cells

Yangyang Kong[a], Tingjuan Huang[a], Haiyan Zhang[a,b,c], Qianqian Zhang[a,b,c], Junjie Ren[a], Xiaohong Guo[a,b,c], Huiqin Fan[a,b,c], Lixin Liu[a,b,c,*]

[a] Department of Gastroenterology and Hepatology, The First Clinical Hospital of Shanxi Medical University, Taiyuan, 030001, China
[b] Experimental Center of Science and Research, The First Clinical Hospital of Shanxi Medical University, Taiyuan, 030001, China
[c] Key Laboratory of Cell Physiology, Provincial Department of the Ministry of Education, Shanxi Medical University, Taiyuan, 030001, China

ARTICLE INFO

Keywords:
LncRNA NEAT1/miR-29b/Atg9a axis
Insulin-like growth factor binding protein-related protein 1
Hepatic stellate cells
Autophagy
Liver fibrosis

ABSTRACT

Aims: Insulin-like growth factor binding protein-related protein 1 (IGFBPrP1) promotes hepatic stellate cell (HSC) autophagy and activation. However, the underlying mechanism remains unknown. Noncoding RNAs (ncRNAs) including long noncoding RNAs (lncRNAs) and microRNAs (miRNAs), have received increasing attention. We aimed to investigate the roles of the lncRNA nuclear enriched abundant transcript 1 (NEAT1), miR-29b, and autophagy related protein 9a (Atg9a), and their relationships with each other during IGFBPrP1-induced HSC autophagy and activation.

Main methods: Levels of NEAT1, miR-29b, Atg9a, and autophagy were detected in adenovirus-mediated IGFBPrP1 (AdIGFBPrP1)-treated mouse liver tissue and immortalized mouse hepatic stellate cell line JS1 transfected with either AdIGFBPrP1 or siIGFBPrP1. In AdIGFBPrP1-treated JS1 cells, autophagy and activation were detected after altering NEAT1, miR-29b, or Atg9a levels. In AdIGFBPrP1-treated JS1 cells, relationships among NEAT1, miR-29b, and Atg9a were explored using dual-luciferase reporter assays, Western blot, qRT-PCR, and immunofluorescence.

Key findings: IGFBPrP1 increased levels of NEAT1, Atg9a, and autophagy while decreasing the level of miR-29b in mouse liver tissues and mouse HSCs. Moreover, NEAT1 increased HSC autophagy and activation while miR-29b decreased both processes. Atg9a also participated in IGFBPrP1-induced HSC autophagy and activation. Importantly, NEAT1, miR-29b, and Atg9a formed a NEAT1/miR-29b/Atg9a regulatory axis for IGFBPrP1-induced HSC autophagy and activation.

Significance: Our study unveiled the new NEAT1/miR-29b/Atg9a regulatory axis involved in IGFBPrP1-induced mouse HSC autophagy and activation. The study thus provides new insights in the pathogenesis and potential therapeutic strategies of liver fibrosis.

1. Introduction

Liver fibrosis is a reversible wound-healing response and the final common pathway of chronic hepatic diseases with a prevalence of 2%–19% [1,2]. Upon prolonged liver injury in chronic hepatic diseases, liver fibrosis may develop into cirrhosis and hepatocellular carcinoma [3], making liver fibrosis a major public health concern.

The activation of hepatic stellate cells (HSCs) plays a key role in liver fibrosis. During this process, levels of the HSC activation marker alpha-smooth muscle actin (α-SMA) and the major extracellular matrix (ECM) component collagen type I (collagen I) increase [3]. Additionally, many cytokines participate in HSC activation and liver fibrosis, the most profibrotic of which is transforming growth factor beta 1 (TGFβ1) [4]. Furthermore, our previous studies have shown that insulin-like growth factor binding protein-related protein 1 (IGFBPrP1) accelerates liver fibrosis and interacts with TGFβ1 [4–6]. However, the underlying mechanism of liver fibrosis induced by IGFBPrP1 remains unclear.

Autophagy is a self-digestive process used to balance cellular energy metabolism and that releases lipid to promote HSC activation [7]. Autophagy involves many proteins, including microtubule-associated protein 1 light chain 3B (LC3B), p62 and a series of autophagy related

* Corresponding author. Department of Gastroenterology and Hepatology and Experimental Center of Science and Research, The First Clinical Hospital of Shanxi Medical University; Key Laboratory of Cell Physiology, Provincial Department of the Ministry of Education, Shanxi Medical University, 85 Jiefang South Road, Taiyuan, 030001, Shanxi Province, China.
E-mail address: lixinliu6@hotmail.com (L. Liu).

https://doi.org/10.1016/j.lfs.2019.116902
Received 26 July 2019; Received in revised form 13 September 2019; Accepted 20 September 2019
Available online 11 October 2019
0024-3205/

(Atg) proteins. During autophagy, LC3B–I is converted to LC3B-II. p62, or SQSTM1, is an autophagy substrate [8]. Atg9 is the only integral membrane protein [9] and has two functional orthologues, Atg9a and Atg9b. Atg9a is widely expressed while Atg9b is only expressed in the placenta and pituitary gland [10].

Given their important roles in many biological processes, increased attention has been paid to noncoding RNAs (ncRNAs). One type of ncRNA is the microRNA (miRNA), a short ncRNA that induces mRNA degradation or represses mRNA translation by targeting the 3′-untranslated region (3′-UTR) of mRNAs [11]. The miR-29 family includes miR-29a, miR-29b and miR-29c, which all have the same seed region and are downregulated during liver fibrosis. Importantly, miR-29b is highly expressed in HSCs compared to other hepatic cell types [12], suggesting an HSC-specific function. Therefore, we focused on miR-29b for our study. Atg9a is a predicted target of miR-29b, however, the exact relationships between miR-29b and Atg9a in liver fibrosis is unknown.

miRNAs do not independently participate in physiological and pathological processes. Instead, long noncoding RNAs (lncRNAs) regulate miRNAs, thus ultimately regulating target mRNA levels [13,14]. Whether there is a lncRNA regulating miR-29b is unknown. Prediction software indicates that the lncRNA nuclear enriched abundant transcript 1 (NEAT1) contains a target site for miR-29b. In addition, NEAT1 is highly expressed in fibrotic liver tissue and activated HSCs [15]. However, whether NEAT1 regulates miR-29b in liver fibrosis is still unknown.

TGFβ1 has been reported to stimulate HSC autophagy [16], suppress miR-29b expression [12], and is related to NEAT1 and Atg9a in HSCs [15,17]. We previously demonstrated that IGFBPrP1 promotes HSC activation via stimulating HSC autophagy [18]. However, whether IGFBPrP1 affects NEAT1, miR-29b, and Atg9a remains elusive, and if so, the roles of NEAT1, miR-29b, and Atg9a, and their relationships with each other during IGFBPrP1-induced HSC autophagy and activation need to be further explored.

2. Materials and methods

2.1. Animals

We have previously established a model of AdIGFBPrP1-induced liver fibrosis [18], which was used for *in vivo* experiments in this study. Male C57BL/6 mice, 5–6 weeks old, were purchased from the Institute of Laboratory Animals at the Military Academy of Medical Sciences (Beijing, China). The mice were transfected with adenovirus-mediated IGFBPrP1 [AdIGFBPrP1 (Sangon Biotech, Shanghai, China)] via the tail vein. Animal experiments complied with the National Institutes of Health guide for the care and use of laboratory animals. A total of 120 C57BL/6 mice were randomly divided into the AdIGFBPrP1 group (n = 40), to which 0.1 mL AdIGFBPrP1 (2×10^9 pfu/mouse) was injected via the tail vein, the CAd group (n = 40), to which 0.1 mL control adenovirus (adenoviral vectors carrying no cDNA, 2×10^9 pfu/mouse) was injected via the tail vein, or the control group (n = 40), to which 0.1 mL saline was injected via the tail vein. At weeks 1 (n = 8), 2 (n = 8), 4 (n = 8), 8 (n = 8), 12 (n = 8) after adenoviral transfection, the mouse liver tissues stored at −80 °C for further analysis.

2.2. Hematoxylin and eosin staining (H&E staining)

Mouse liver tissue was fixed for 24 h with 10% formalin and then embedded in paraffin. Liver tissues were sectioned to 4 μm thickness and stained with hematoxylin and eosin. Liver tissue images were collected using a microscope (BX43, Olympus, Tokyo, Japan) at 200× magnification.

2.3. Sirius red staining

Paraffin-embedded liver tissues were cut into 4-μm-thick sections, routinely dewaxed and hydrated, then stained with 2% Brilliant Green (Solarbio, Beijing, China) for 15 min and washed with distilled water. Next, tissues were stained with 0.1% saturated picric acid-Sirius red solution (Solarbio) for 20 min then washed with distilled water. Tissue images were then collected with a microscope (BX43, Olympus) at 200× magnification. The red areas represented collagen fibers and were semi-quantified by image analysis using Image-Pro Plus 7.0 software.

2.4. Cell culture

The immortalized mouse hepatic stellate cell line JS1 (BeNa Culture Collection, Suzhou, China) was cultured with Dulbecco's modified Eagle's medium (DMEM, Biological Industries, USA) containing 10% fetal bovine serum (FBS, Biological Industries) and 1% 100 × penicillin/streptomycin (TransGen Biotech, Beijing, China). JS1 cells were cultured at 37 °C in an atmosphere in 5% CO_2 atmosphere.

2.5. Cell transfection

JS1 cell transfection was used for the experiments in sections 3.2, 3.3 and 3.4. Approximately 1×10^5 JS1 cells were seeded in each well of a 6-well plate containing 2 mL DMEM with 10% FBS. For experiments with IGFBPrP1 overexpression, the cells were divided into the AdIGFBPrP1 group by transfection with AdIGFBPrP1, the CAd group by transfection with control adenovirus (adenoviral vectors carrying no cDNA), or the control group by culturing with only DMEM containing 10% FBS. Cells were then collected at 6 h (n = 3), 12 h (n = 3), 24 h (n = 3), 48 h (n = 3), and 72 h (n = 3) after adenoviral transfection.

For experiments of involving IGFBPrP1 knockdown, JS1 cells were divided into three groups. The control group was cultured for a total of 48 h in DMEM containing 10% FBS. The EBSS group was cultured in DMEM containing 10% FBS for 44 h then in Earle's Balanced Salt Solution (EBSS, Solarbio) for 4 h. The EBSS + siRNA-NC group was cultured with control siRNA for 44 h followed by incubation in EBSS for 4 h. The EBSS + siIGFBPrP1 group was incubated with 50 nM siIGFBPrP1 (Sangon Biotech) using LipoFiter 3.0™ (Hanbio, Shanghai, China) for 44 h followed by incubation in EBSS for 4 h.

The NEAT1 overexpression plasmid (NEAT1), siNEAT1, siAtg9a, miR-29b mimics, and miR-29b inhibitors were designed and synthesized by Sangon Biotech. Vector-NC, siRNA-NC, mimics-NC, or inhibitors-NC were used as the corresponding negative controls. JS1 cells were transfected with NEAT1, siNEAT1, siAtg9a, miR-29b mimics, or miR-29b inhibitors using LipoFiter 3.0™. NEAT1 was used at a concentration of 4 μg per well while siNEAT1, siAtg9a, and miR-29b mimics were used at a final concentration of 50 nM and miR-29b inhibitors were used at a final concentration of 100 nM.

The sequences of siIGFBPrP1, siNEAT1, siAtg9a, and the miR-29b mimics and inhibitors are listed in Supplementary Table 1.

2.6. Western blot

Proteins from liver tissue and JS1 cells were extracted using a total protein extraction kit (KeyGEN Biotech, Nanjing, China). Total protein levels were quantified using the BCA Protein Assay Kit (KeyGEN Biotech). 80 μg total protein of each sample was loaded per well and the samples were normalized. Whole extracts were separated using sodium dodecyl sulfate-polyacrylamide gel electrophoresis and then transferred onto Polyvinylidene fluoride membranes (Millipore, Bedford, MA, USA). Membranes were then incubated with primary antibodies targeting IGFBPrP1, α-SMA, collagen I, LC3B, SQSTM1/p62 or Atg9a (Abcam, Cambridge, UK) at a 1:1000 dilution or β-actin (TransGen Biotech) at 1:2500, which was used as an internal control. Membranes

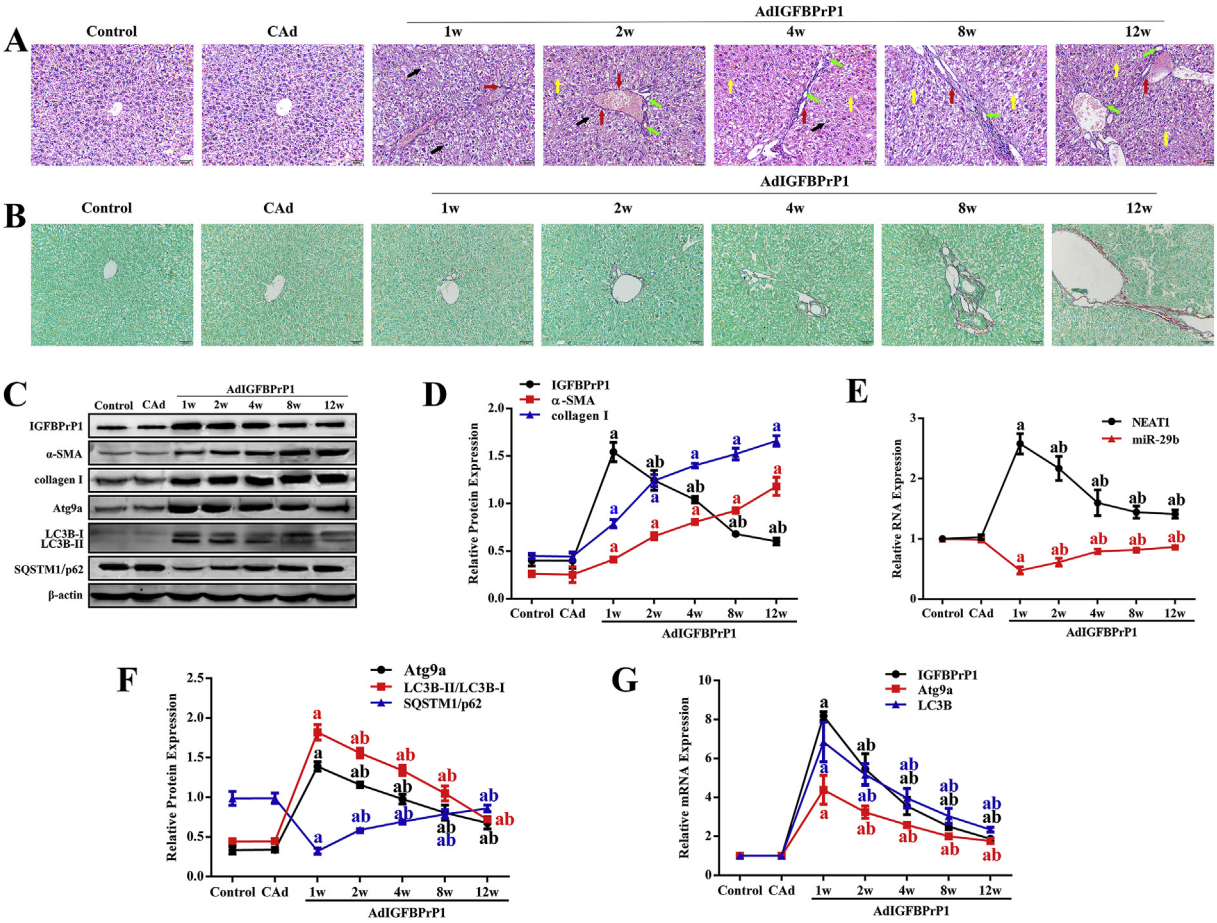

Fig. 1. Levels of NEAT1, miR-29b, Atg9a, and autophagy in AdIGFBPrP1-induced mouse liver fibrosis. (A) Histological changes in liver tissues were observed via H&E staining (magnification 200×). Black arrows indicate hydropic degeneration or steatosis. Yellow arrows indicate necrosis. Red arrows show infiltration of inflammatory cells. Green arrows represent bile duct proliferation. (B) Sirius red staining of liver tissues. The red areas represent collagen fibrils. (magnification 200×). (C) Western blot analysis examining protein expression levels of IGFBPrP1, α-SMA, collagen I, Atg9a, LC3B-II, LC3B–I, SQSTM1/p62 in Control, CAd, and AdIGFBPrP1 groups after 1, 2, 4, 8, and 12 w of treatment in mouse liver tissues. (D) Line graph showing relative protein expression levels of IGFBPrP1, α-SMA, and collagen I in mouse liver tissues. β-actin was used as an internal control. (E) Line graph showing the qRT-PCR analysis of NEAT1 and miR-29b RNA levels in Control, CAd, and AdIGFBPrP1 groups after 1, 2, 4, 8, and 12 w of treatment in mouse liver tissues. (F) Line graph showing the relative protein expression levels of Atg9a, LC3B-II/LC3B–I, and SQSTM1/p62 in mouse liver tissues. β-actin was used as an internal control. (G) Line graph of qRT-PCR analysis for IGFBPrP1, Atg9a, and LC3B mRNA levels in Control, CAd, and AdIGFBPrP1 groups after 1, 2, 4, 8, and 12 w of treatment in mouse liver tissues. Data are presented as mean ± SD (n = 8 per group). [a] $P < 0.05$ vs Control group. [b] $P < 0.05$ vs AdIGFBPrP1 1w group. (For interpretation of the references to colour in this figure legend, the reader is referred to the Web version of this article.)

were then incubated with secondary antibodies for 2 h at room temperature.

2.7. Quantitative real-time polymerase chain reaction (qRT-PCR)

Total RNA was extracted from liver tissue and JS1 cells using the miRNeasy Mini Kit (Qiagen, Valencia, CA, USA). Per sample, 1 μg RNA was reverse transcribed to cDNA using the miScript II RT Kit (Qiagen) and RNA expression levels measured by qRT-PCR using the miScript SYBR® Green PCR Kit (Qiagen). GAPDH levels were used to normalize the relative abundance of NEAT1 and mRNAs. U6 levels were used to normalize the relative abundance of miR-29b. Expression levels of both GAPDH and U6 were stable among groups. Primers were designed and synthesized by Sangon Biotech and are listed in Supplementary Table 1.

2.8. Immunofluorescence

JS1 cells were cultured in 24-well plates and fixed with 4% paraformaldehyde for 10 min, permeabilized with 0.1% Triton X-100 for 15 min, then blocked with 1% BSA for 1 h at room temperature. Next, cells were incubated with the rabbit monoclonal Atg9a antibody (1:100) overnight at 4 °C followed by incubation with Alexa Fluor 594-conjugated Donkey Anti-Rabbit IgG (H + L) secondary antibody (1:500, Proteintech, Chicago, IL, USA). A 5 μg/mL DAPI solution (Solarbio) was used to stain nuclei. Images (Scale bar, 20 μm) were taken using a fluorescence microscope (BX43, Olympus).

2.9. Dual-luciferase reporter assay

The wild type 3′UTR sequence of Atg9a, which contains the miR-29b binding site (Atg9a Wt), and a mutant Atg9a sequence (Atg9a Mut) were synthesized (Sangon Biotech) and cloned into the pmirGLO vector (Promega, USA). The sequences of Atg9a Wt and Atg9a Mut are listed in Supplementary Table 1. JS1 cells were cultured in 24-well plates then transfected with pmirGLO-Atg9a Wt or pmirGLO-Atg9a Mut followed by treatment with either 50 nM miR-29b mimics or mimics-NC using LipoFiter 3.0™. Relative luciferase activity was measured using dual-Luciferase® Reporter Assay System (Promega) according to the manufacturer's protocol [19].

The wild type sequence of NEAT1, which contains the miR-29b binding site (NEAT1 Wt), and a mutant version of this sequence (NEAT1 Mut) were synthesized by Sangon Biotech and inserted into the

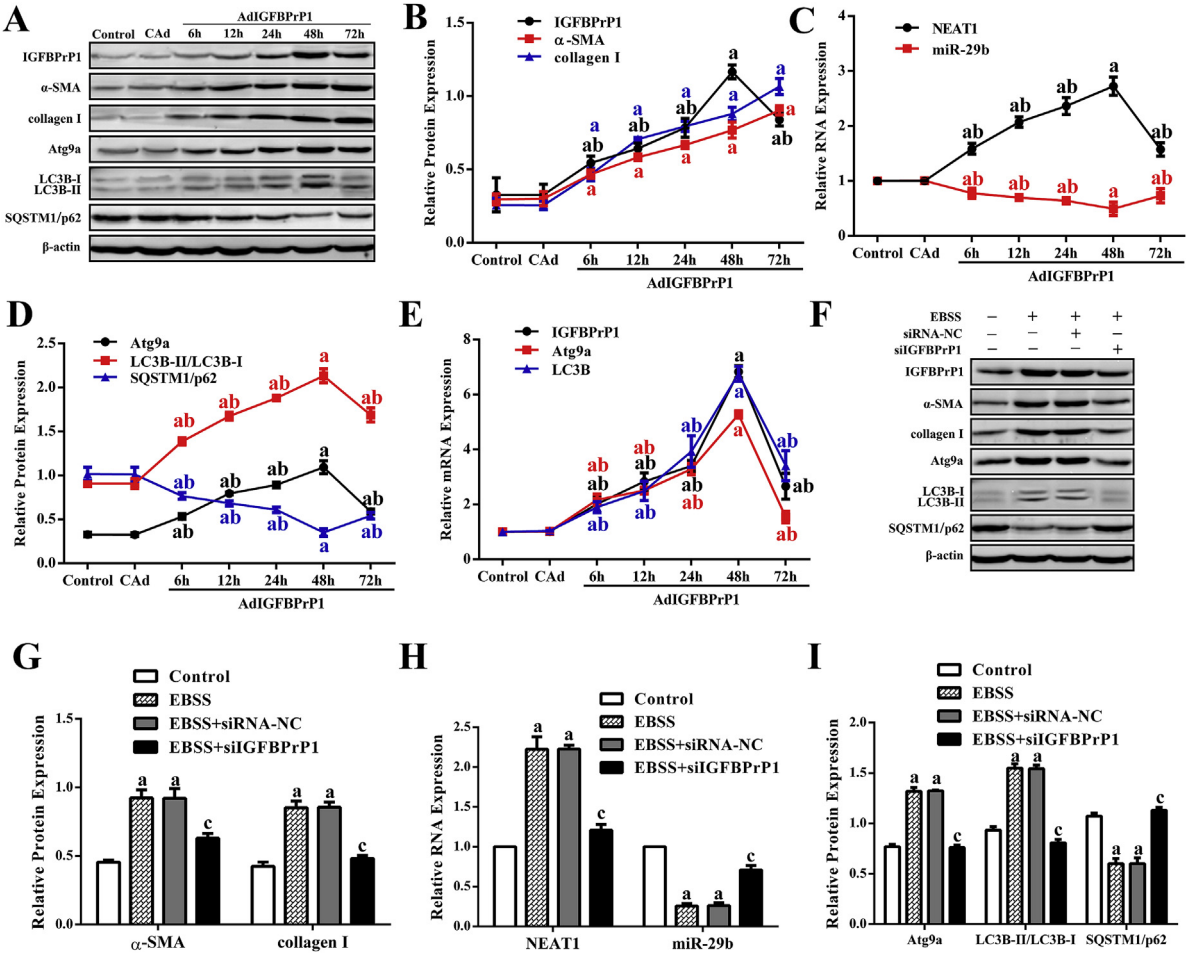

Fig. 2. Levels of NEAT1, miR-29b, Atg9a, and autophagy in JS1 cells treated with AdIGFBPrP1 or siIGFBPrP1. (A) Western blot analysis of IGFBPrP1, α-SMA, collagen I, Atg9a, LC3B-II, LC3B–I, and SQSTM1/p62 expression levels in Control, CAd, and AdIGFBPrP1 groups after 6, 12, 24, 48, and 72 h of treatment in JS1 cells. (B) Line graph showing relative protein expression levels of IGFBPrP1, α-SMA, and collagen I in Control, CAd, and AdIGFBPrP1 groups after 6, 12, 24, 48, and 72 h of treatment in JS1 cells. β-actin was used as an internal control. (C) Line graph showing qRT-PCR analysis of NEAT1 and miR-29b RNA expression levels in Control, CAd, and AdIGFBPrP1 groups after 6, 12, 24, 48, and 72 h of treatment in JS1 cells. (D) Line graph showing relative protein expression levels of Atg9a, LC3B-II/LC3B–I, and SQSTM1/p62 in JS1 cells. β-actin was used as an internal control. (E) Line graph showing qRT-PCR analysis of IGFBPrP1, Atg9a, and LC3B mRNA levels in Control, CAd, and AdIGFBPrP1 groups after 6, 12, 24, 48, and 72 h of treatment in JS1 cells. Data are presented as mean ± SD (n = 3 per group). [a] $P < 0.05$ vs Control group. [b] $P < 0.05$ vs AdIGFBPrP1 48 h group. (F) Western blot analysis of IGFBPrP1, α-SMA, collagen I, Atg9a, LC3B-II, LC3B–I, and SQSTM1/p62 protein levels after treatment with siIGFBPrP1 during EBSS-induced starvation conditions in JS1 cells. (G) Relative protein levels of α-SMA and collagen I after treatment of JS1 cells with siIGFBPrP1 during EBSS-induced starvation conditions. β-actin was used as an internal control. (H) qRT-PCR analysis of NEAT1 and miR-29b RNA levels after treatment of JS1 cells with siIGFBPrP1 during EBSS-induced starvation conditions. (I) Relative protein expression levels of Atg9a, LC3B-II/LC3B–I, and SQSTM1/p62 after treatment of JS1 cells with siIGFBPrP1 during EBSS-induced starvation conditions. β-actin was used as an internal control. Data are presented as mean ± SD (n = 3 per group). [a] $P < 0.05$ vs Control group. [c] $P < 0.05$ vs EBSS group.

pmirGLO vector. The sequences of NEAT1 Wt and NEAT1 Mut are listed in Supplementary Table 1. NEAT1 binding of miR-29b was evaluated as done for testing Atg9a binding to miR-29b [15].

2.10. Nuclear-cytoplasmic fractionation

In order to confirm the cellular localization of NEAT1, the PARIS™ Kit (Invitrogen, Carlsbad, CA, USA) was used following the manufacturer's instructions to separate nuclear and cytoplasmic RNA from JS1 cells treated with AdIGFBPrP1 for 48 h. All fractionation steps were performed at 4 °C or on ice. Approximately 1×10^7 JS1 cells were trypsinized and pelleted, and then mixed with cell fractionation buffer and centrifuged samples for 3 min at 500 g. The supernatant, which represents the cytoplasmic fraction, was then collected. The nuclear pellet was then washed with cell fractionation buffer and re-pelleted 1 min at 500 g. Add cell disruption buffer to the nuclear pellet. Mix the lysate or the cytoplasmic fraction with 2 × lysis/binding solution then add equal volume of 100% ethanol to the mixture. The mixture was then drawn through a filter cartridge then Wash with wash solution 1 and wash solution 2/3. Nuclear or cytoplasmic RNA was then eluted with elution solution. The GAPDH and U6 were used as the cytoplasmic and nuclear controls, respectively [20].

2.11. Statistical analysis

Statistical analysis was performed using SPSS 22.0 software. Data were expressed as mean ± SD. Factorial design analysis of variance or one-way analysis of variance was used to compare different groups. LSD-t was used for multiple comparisons. $P < 0.05$ was considered statistically significant.

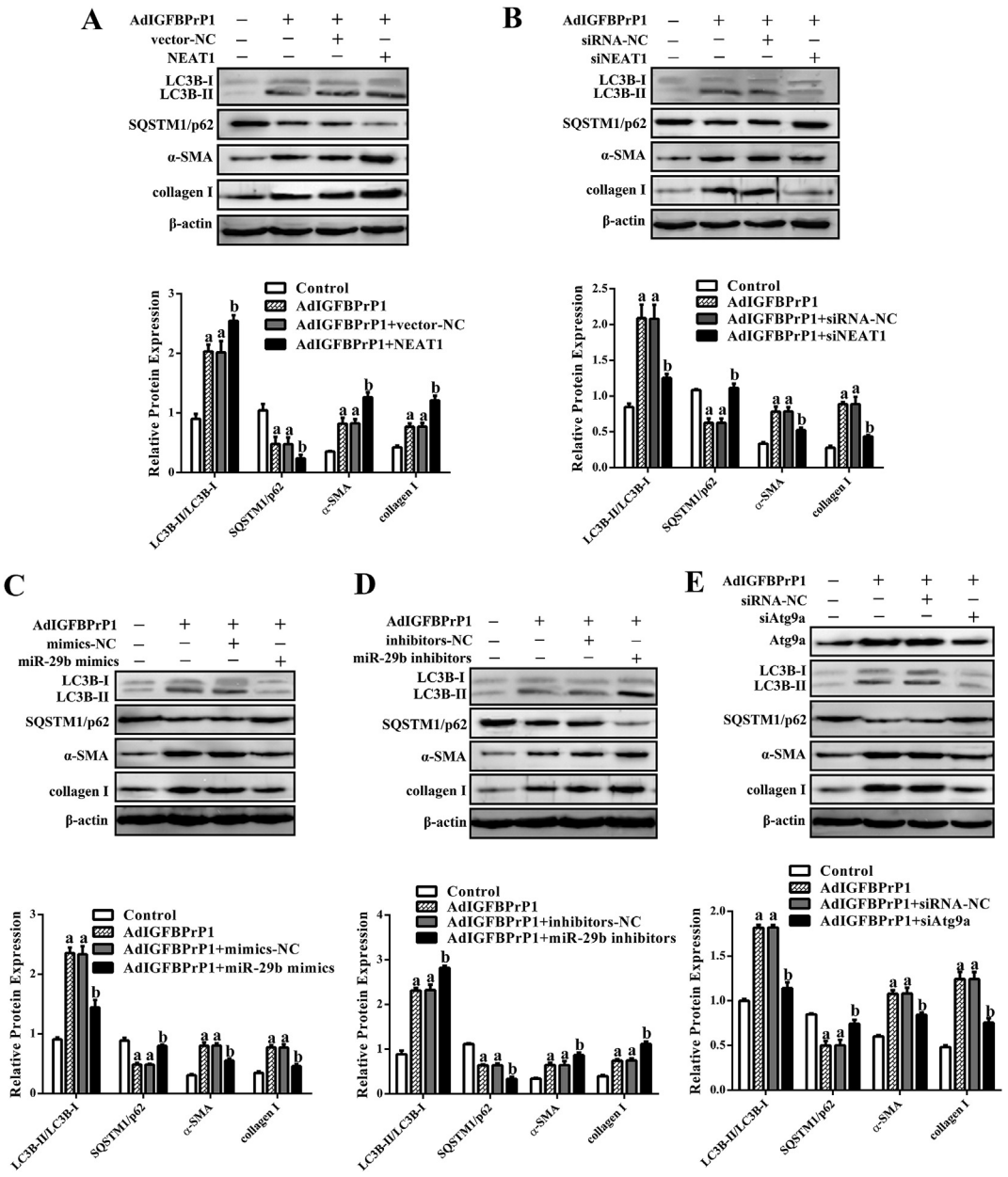

Fig. 3. Effects of NEAT1, miR-29b, and Atg9a on HSC autophagy and activation in AdIGFBPrP1-treated JS1 cells. (A–B) Western blot analysis of LC3B-II, LC3B–I, SQSTM1/p62, α-SMA, and collagen I protein levels in AdIGFBPrP1-treated JS1 cells transfected with NEAT1 or siNEAT1. (C–D) Western blot analysis of LC3B-II, LC3B–I, SQSTM1/p62, α-SMA, and collagen I protein levels in AdIGFBPrP1-treated JS1 cells transfected with miR-29b mimics or miR-29b inhibitors. (E) Western blot analysis of Atg9a, LC3B-II, LC3B–I, SQSTM1/p62, α-SMA, and collagen I protein levels and relative protein expression of LC3B-II/LC3B–I, SQSTM1/p62, α-SMA, and collagen I in AdIGFBPrP1-treated JS1 cells transfected with siAtg9a. Data are presented as mean ± SD (n = 3 per group). [a] $P < 0.05$ vs Control group, [b] $P < 0.05$ vs AdIGFBPrP1 group.

3. Results

3.1. Levels of NEAT1, miR-29b, Atg9a and autophagy during AdIGFBPrP1-induced liver fibrosis in mice

We investigated the levels of NEAT1, miR-29b, Atg9a, and autophagy during AdIGFBPrP1-induced liver fibrosis in mice. H&E staining showed an increase in hydropic degeneration, steatosis, necrosis, infiltration of inflammatory cells and bile duct proliferation in IGFBPrP1-treated liver tissue (Fig. 1A). Sirius red staining showed a gradual increase in the amount of collagen fibrils in liver tissue from 1 w to 12 w after AdIGFBPrP1 was transfected into liver tissue (Fig. 1B and Supplementary Fig. 1A). As shown in Fig. 1C, D, G and Supplementary Figs. 1B and E, Western blot and qRT-PCR showed increases in IGFBPrP1 levels, demonstrating the successful transfection of IGFBPrP1 into liver tissues. Western blot revealed increases in α-SMA and collagen I levels over time (Fig. 1C-D and Supplementary Fig. 1B). H&E staining, Sirius red staining and Western blot analysis of α-SMA and collagen I levels confirmed the occurrence of liver fibrosis. qRT-PCR analysis showed that overexpression of IGFBPrP1 significantly upregulated NEAT1 expression while downregulating miR-29b levels (Fig. 1E and Supplementary Fig. 1C). In addition, Western blot and qRT-PCR analysis indicated increases in Atg9a and the LC3B-II/LC3B–I ratio (or LC3B mRNA) and decreases in SQSTM1/p62 levels (Fig. 1C, F, G and Supplementary Figs. 1D–E). In addition, after AdIGFBPrP1 treatment, levels of IGFBPrP1, NEAT1, Atg9a and autophagy synchronously increased and peaked at 1 w and then gradually decreased from 2 w to 12 w, but levels remained higher than those of the control group,

while miR-29b levels showed the opposite trend (Fig. 1D–G). These results suggest that NEAT1, Atg9a and autophagy increase and miR-29b decreases during AdIGFBPrP1-induced liver fibrosis.

3.2. Levels of NEAT1, miR-29b, Atg9a, and autophagy in JS1 cells transfected with AdIGFBPrP1 or siIGFBPrP1

To identify whether IGFBPrP1 affects levels of NEAT1, miR-29b, Atg9a, and autophagy in HSCs, whose activation is the central link of liver fibrosis, we transfected JS1 cells with AdIGFBPrP1 and showed upregulation of IGFBPrP1 mRNA and protein (Fig. 2A, B, E and Supplementary Figs. 2A and D), indicating the successful transfection of IGFBPrP1. Western blots showed that α-SMA and collagen I levels increased after AdIGFBPrP1 transfection (Fig. 2A-B and Supplementary Fig. 2A), demonstrating that IGFBPrP1 promotes HSC activation and ECM deposition. qRT-PCR results showed that NEAT1 expression was promoted while miR-29b expression was reduced by AdIGFBPrP1 in JS1 cells (Fig. 2C and Supplementary Fig. 2B). Overexpression of IGFBPrP1 significantly increased levels of Atg9a protein and the LC3B-II/LC3B–I protein ratio, and decreased levels of SQSTM1/p62 (Fig. 2A, D and Supplementary Fig. 2C). qRT-PCR analysis also revealed increases in levels of Atg9a and LC3B mRNA (Fig. 2E and Supplementary Fig. 2D). Furthermore, levels of IGFBPrP1, NEAT1, Atg9a, and autophagy synchronously increased from 6 h, peaking at 48 h, then decreasing at 72 h but remaining higher than the control group. The opposite trend was observed for levels of miR-29b (Fig. 2B–E).

To further evaluate the effects of IGFBPrP1 on NEAT1, miR-29b, Atg9a, and autophagy in HSCs, JS1 cells were transfected with siIGFBPrP1 to silence IGFBPrP1 expression, which was confirmed by qRT-PCR and Western blot results (Supplementary Figs. 2E–F). Autophagy is stimulated by several metabolic stresses, including starvation, thus EBSS was employed to trigger starvation-induced autophagy [21]. Silencing IGFBPrP1 decreased protein levels of α-SMA and collagen I (Fig. 2F-G). Additionally, qRT-PCR indicated that silencing IGFBPrP1 expression reversed starvation-induced upregulation of NEAT1 and downregulation of miR-29b during EBSS treatment (Fig. 2H). Finally, Western blot showed that the loss of IGFBPrP1 decreased both Atg9a levels and the LC3B-II/LC3B–I ratio, and increased SQSTM1/p62 levels, compared to levels in the EBSS-only treated group (Fig. 2F, I).

These results suggest that IGFBPrP1 promotes NEAT1, Atg9a, and autophagy and suppresses miR-29b while silencing IGFBPrP1 had the opposite effects.

3.3. Effects of NEAT1, miR-29b, and Atg9a on IGFBPrP1-induced HSC autophagy and activation in JS1 cells

To further investigate whether NEAT1 has an effect on HSC autophagy and activation, NEAT1 was overexpressed or knocked down in AdIGFBPrP1-treated JS1 cells. First, qRT-PCR confirmed increases or decreases in NEAT1 RNA levels after transfection with either NEAT1 or siNEAT1, respectively, compared to the AdIGFBPrP1-treated group (Supplementary Figs. 3A–B), confirming that NEAT1 overexpression or RNAi was effective. Next, western blotting showed that NEAT1 overexpression increased LC3B-II/LC3B–I ratio, α-SMA levels, and collagen I levels while decreasing expression of SQSTM1/p62 compared to the AdIGFBPrP1-only treated group (Fig. 3A). Knockdowns of NEAT1 triggered the opposite effects (Fig. 3B). These results support a positive regulatory effect of NEAT1 on autophagy and activation in AdIGFBPrP1-treated JS1 cells.

Next, we evaluated the role of miR-29b by using miR-29b mimics or inhibitors to alter miR-29b levels whose effects were experimentally confirmed (Supplementary Figs. 3C–D). We then used western blotting to examine levels of LC3B-II/LC3B–I, SQSTM1/p62, α-SMA, and collagen I after co-transfecting JS1 cells with both AdIGFBPrP1 and either miR-29b mimics or inhibitors. Our results showed that miR-29b mimics decreased the LC3B-II/LC3B–I ratio and levels of both α-SMA and collagen I while increasing SQSTM1/p62 levels compared to the AdIGFBPrP1-only treated group (Fig. 3C). As expected, co-transfection with the miR-29b inhibitors increased the LC3B-II/LC3B–I ratio and levels of α-SMA and collagen I while decreasing the level of SQSTM1/p62 (Fig. 3D). These results thus suggest that miR-29b negatively regulates autophagy and activation in AdIGFBPrP1-treated JS1 cells.

We also investigated the role of Atg9a by transfecting AdIGFBPrP1-treated JS1 cells with siAtg9a, which successfully reduced levels of Atg9a mRNA and protein (Fig. 3E and Supplementary Fig. 3E). Western blots showed that knocking down Atg9a suppressed LC3B-II/LC3B–I, α-SMA, and collagen I levels while increasing SQSTM1/p62 expression compared to levels in the AdIGFBPrP1 group (Fig. 3E). These results indicate that Atg9a is involved in HSC autophagy and activation induced by IGFBPrP1.

3.4. The NEAT1/mir-29b/Atg9a axis regulates HSC autophagy and activation in AdIGBPrP1-treated JS1 cells

We further explored the relationships among NEAT1, miR-29b, and Atg9a in IGFBPrP1-induced HSC autophagy and activation. We first attempted to identify the target of miR-29b. We used the prediction software TargetScan to predict miR-29b targets and results indicated that Atg9a is a possible miR-29b target (Fig. 4A). PmirGLO was used to generate an Atg9a luciferase reporter containing a miR-29b binding site (Atg9a Wt) or a mutated binding site (Atg9a Mut). miR-29b mimics significantly suppressed the luciferase activity of Atg9a Wt while miR-29b mimics had no effect on the activity of Atg9a Mut (Fig. 4B), indicating that Atg9a is a target of miR-29b. As shown in Fig. 4C–F, after transfecting AdIGFBPrP1-treated JS1 cells with either miR-29b mimics or inhibitors, we found that miR-29b mimics downregulated Atg9a protein levels while miR-29b inhibitors enhanced Atg9a expression. Immunofluorescence results showed that miR-29b mimics or inhibitors either decreased or increased Atg9a levels, respectively, compared to levels in the AdIGFBPrP1 group (Fig. 4G). Furthermore, western blotting indicated that siAtg9a decreased the LC3B-II/LC3B–I ratio and levels of α-SMA and collagen I while increasing SQSTM1/p62 levels compared to levels of AdIGFBPrP1 + miR-29b inhibitors group (Fig. 4H-I), demonstrating that silencing Atg9a alleviated the HSC autophagy and activation induced by the miR-29b inhibitors. Taken together, the results indicate that miR-29b directly regulates Atg9a expression to regulate autophagy and activation in HSCs transfected with IGFBPrP1.

To determine whether miR-29b is involved in NEAT1-induced autophagy and activation of HSCs, we used RNAhybrid software and found NEAT1 contains a complementary sequence for miR-29b (Fig. 5A). Dual-luciferase reporter assays revealed that miR-29b mimics decreased the luciferase activity of NEAT1 Wt and had no effects on the luciferase activity of NEAT1 Mut (Fig. 5B), demonstrating that NEAT1 directly binds to miR-29b. We also saw a dramatic reduction of miR-29b levels in the NEAT1-overexpression group (Fig. 5C). When NEAT1 was knocked down, opposing trends were observed (Fig. 5D). Furthermore, western blots showed that the upregulation of miR-29b reversed the increase in HSC autophagy and activation triggered by NEAT1 (Fig. 5E-F). In addition, immunofluorescence results demonstrated that miR-29b mimics decreased Atg9a expression compared to levels of the AdIGFBPrP1 + NEAT1 group (Fig. 5G). Furthermore, as showed in Fig. 5H, RNA nuclear-cytoplasmic fractionation showed that NEAT1 is located both in the nucleus and the cytoplasm, indicating that NEAT1 may regulate miR-29b located in cytoplasm [22]. These results thus suggest that NEAT1 stimulates IGFBPrP1-induced HSC autophagy and activation by directly suppressing miR-29b. Finally, we determined that silencing Atg9a, the target of miR-29b, reduced the LC3B-II/LC3B–I ratio, decreased α-SMA, and collagen I protein and enhanced SQSTM1/p62 expression relative to levels in the AdIGFBPrP1 + NEAT1 group (Fig. 5I-J). However, we were not able to identify the direct target between NEAT1 and Atg9a, thus NEAT1 may not directly regulate Atg9a and may, instead, indirectly regulate Atg9a via miR-29b. In

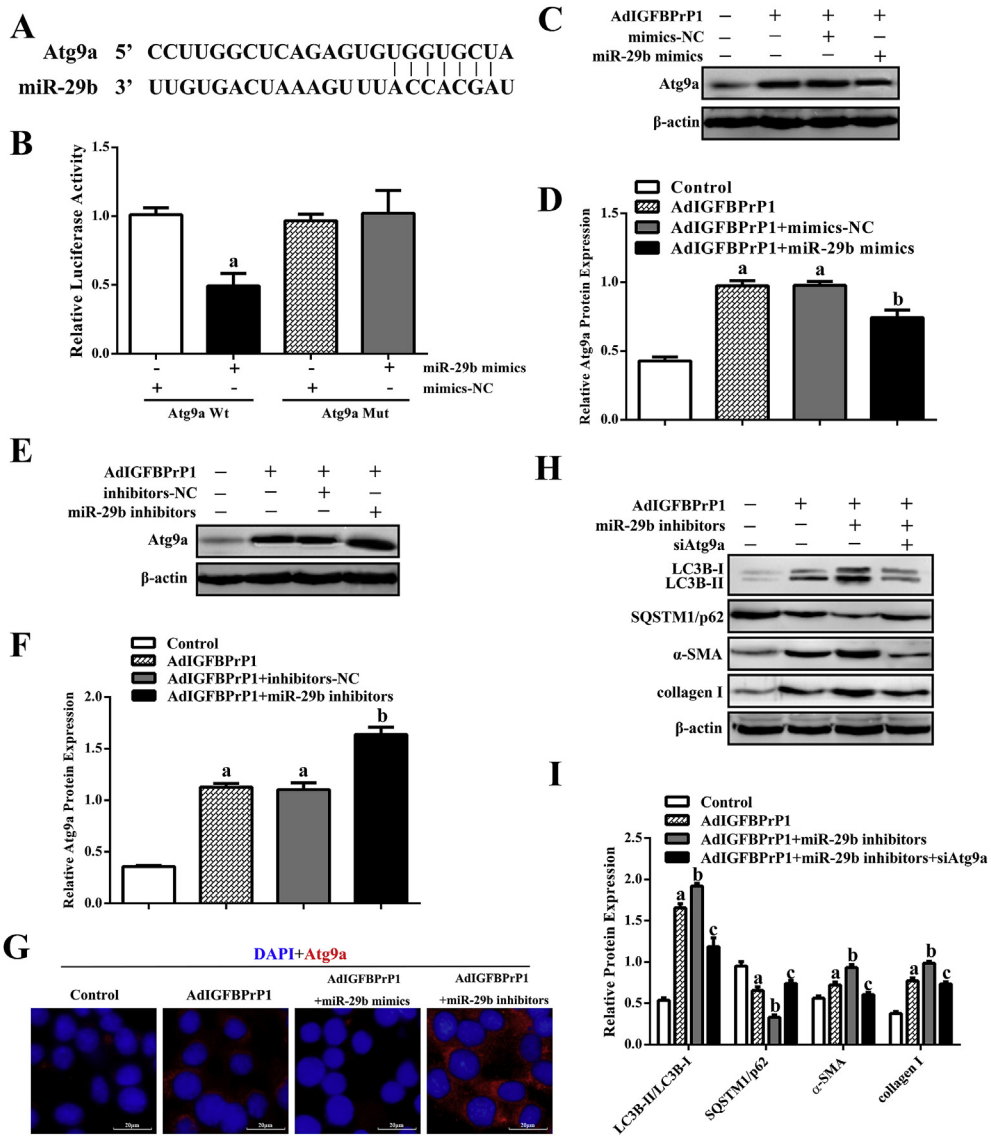

Fig. 4. The miR-29b/Atg9a axis regulates IGFBPrP1-induced HSC autophagy and activation in JS1 cells. (A) The TargetScan (http://www.targetscan.org/) bioinformatic tool predicts that Atg9a is a target of miR-29b. (B) Relative luciferase activity levels in Atg9a Wt + mimics-NC, Atg9a Wt + miR-29b mimics, Atg9a Mut + mimics-NC, and Atg9a Mut + miR-29b mimics groups of JS1 cells. Data are presented as mean ± SD (n = 3 per group). [a] $P < 0.05$ vs Atg9a Mut + mimics-NC group. (C–F) Western blot analysis of Atg9a protein levels in AdIGFBPrP1-treated JS1 cells transfected with miR-29b mimics or inhibitors. Data are presented as mean ± SD (n = 3 per group). [a] $P < 0.05$ vs Control group, [b] $P < 0.05$ vs AdIGFBPrP1 group. (G) Immunofluorescence of Atg9a in AdIGFBPrP1-treated JS1 cells transfected with miR-29b mimics or inhibitors. JS1 cells were stained for Atg9a (red) and DAPI (blue). Scale bar, 20 μm. (H–J) Western blot analysis of LC3B-II, LC3B–I, SQSTM1/p62, α-SMA, and collagen I protein levels in AdIGFBPrP1-treated JS1 cells transfected with miR-29b inhibitors + siAtg9a. Data are presented as mean ± SD (n = 3 per group). [a] $P < 0.05$ vs Control group, [b] $P < 0.05$ vs AdIGFBPrP1 group, [c] $P < 0.05$ vs AdIGFBPrP1 + miR-29b inhibitors group. (For interpretation of the references to colour in this figure legend, the reader is referred to the Web version of this article.)

summary, NEAT1, miR-29b, and Atg9a form the NEAT1/miR-29b/Atg9a regulatory axis to help modulate IGFBPrP1-induced HSC autophagy and activation.

4. Discussion

A growing amount of evidence suggests an important role for ncRNAs in liver fibrosis [13]. In addition, NEAT1 is highly expressed while miR-29b levels are reduced during CCl_4-induced liver fibrosis [12,15]. Here, we found that NEAT1 was upregulated while miR-29b was downregulated during IGFBPrP1-induced liver fibrosis. Autophagy releases lipids in HSCs to maintain energy homeostasis in the face of increasing energy demands during liver fibrosis, suggesting that autophagy is essential for HSC activation [7]. Atg9a delivers small vesicles to form autophagosomes in autophagy initiation [10]. Our study showed that IGFBPrP1 increased Atg9a expression, providing evidences that IGFBPrP1 may participate in autophagy initiation. In addition, we reported that IGFBPrP1 overexpression increased levels of autophagy, which is consistent with our previous study [18] and further confirms the positive regulation of autophagy by IGFBPrP1 during liver fibrosis.

Our *in vivo* experiments showed that IGFBPrP1 expression peaked at 1 w, consistent with our previous study [18], and likely arising from an inability of an adenovirus to integrate into the chromosome and because of host immune responses [6]. Interestingly, alterations in expression levels of NEAT1, Atg9a, and autophagy matched those of IGFBPrP1 while miR-29b expression levels showed the opposite trends. These results indicate that IGFBPrP1 may regulate NEAT1, miR-29b, Atg9a, and autophagy in a dose-dependent manner, which is supported by our previous studies [18] and the dose-dependent downregulation of miR-29b by TGFβ1 [23]. Overall, these *in vivo* results indicate that IGFBPrP1 is closely associated with NEAT1, miR-29b, Atg9a, and autophagy during liver fibrosis.

In vitro experiments also demonstrated that IGFBPrP1 promotes NEAT1, Atg9a, and autophagy expression levels while suppressing miR-29b expression, which confirms previous studies showing high levels of NEAT1, Atg9a, and autophagy and downregulation of miR-29b in activated HSCs [12,15,17,18]. However, the highest levels of IGFBPrP1, NEAT1, Atg9a and autophagy and the lowest levels of miR-29b were observed at 48 h after transfection due to characteristics of adenovirus-mediated transfection of cells [4]. Thus, these *in vitro* results further support results obtained *in vivo*. As expected, siIGFBPrP1 had opposing effects on NEAT1, miR-29b, Atg9a, and autophagy compared to effects of AdIGFBPrP1 treatment. These results collectively suggest that IGFBPrP1 is upstream of NEAT1, miR-29b, Atg9a, and autophagy during HSC activation.

We found that NEAT1 promoted IGFBPrP1-induced HSC autophagy

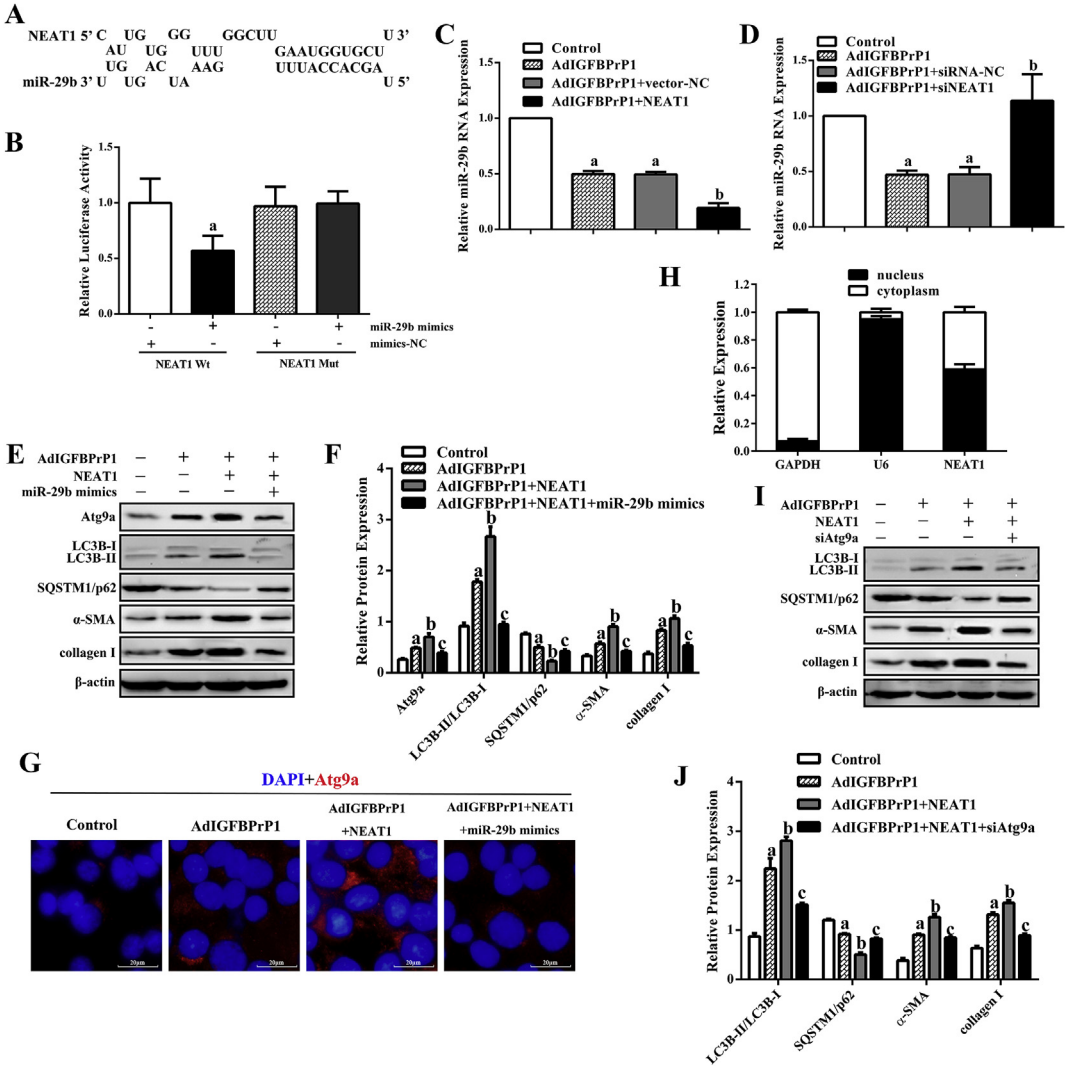

Fig. 5. The NEAT1/miR-29b/Atg9a axis regulates HSC autophagy and activation in AdIGFBPrP1-treated JS1 cells. (A) The RNAhybrid tool (http://bibiserv.techfak.uni-bielefeld.de/rnahybrid/) predicts that NEAT1 contains a complementary sequence for miR-29b. (B) Relative luciferase activities of NEAT1 Wt + mimics-NC, NEAT1 Wt + miR-29b mimics, NEAT1 Mut + mimics-NC, NEAT1 Mut + miR-29b mimics groups of JS1 cells. Data are presented as mean ± SD (n = 3 per group). [a] $P < 0.05$ vs NEAT1 Mut + mimics-NC group. (C–D) qRT-PCR analysis of miR-29b RNA levels in AdIGFBPrP1-treated JS1 cells transfected with NEAT1 or siNEAT1. Data are presented as mean ± SD (n = 3 per group). [a] $P < 0.05$ vs Control group, [b] $P < 0.05$ vs AdIGFBPrP1 group. (E–F) Western blot analysis of Atg9a, LC3B-II, LC3B–I, SQSTM1/p62, α-SMA, and collagen I protein levels in AdIGFBPrP1-treated JS1 cells transfected with NEAT1 + miR-29b mimics. Data are presented as mean ± SD (n = 3 per group). [a] $P < 0.05$ vs Control group, [b] $P < 0.05$ vs AdIGFBPrP1 group, [c] $P < 0.05$ vs AdIGFBPrP1 + NEAT1 group. (G) Immunofluorescence of Atg9a in AdIGFBPrP1-treated JS1 cells transfected with NEAT1 + miR-29b mimics. JS1 cells were stained for Atg9a (red) and DAPI (blue). Scale bar, 20 μm. (H) Localization of NEAT1 in AdIGFBPrP1-treated JS1 cells as identified by RNA nuclear-cytoplasmic fractionation. GAPDH and U6 were separately used as cytoplasmic and nuclear controls. (I–J) Western blot analysis of LC3B-II, LC3B–I, SQSTM1/p62, α-SMA, and collagen I protein levels in AdIGFBPrP1-treated JS1 cells transfected with NEAT1 + siAtg9a. Data are presented as mean ± SD (n = 3 per group). [a] $P < 0.05$ vs Control group, [b] $P < 0.05$ vs AdIGFBPrP1 group, [c] $P < 0.05$ vs AdIGFBPrP1 + NEAT1 group. (For interpretation of the references to colour in this figure legend, the reader is referred to the Web version of this article.)

and activation, which is supported by several previous studies. In support of our results, Ma et al. [24] reported that NEAT1 increases myocardial ischemia reperfusion injury in diabetic rats by promoting myocardial autophagy and Yan et al. [25] found NEAT1 aggravates autophagy in MPTP-induced Parkinson's disease and Yu et al. [15] found that the loss of NEAT1 alleviates HSC activation. In addition, miR-29 also plays important roles in autophagy and HSC activation. For example, miR-29a inhibited autophagy in ulcerative colitis [26] and overexpression of miR-29b reverses TGFβ1-triggered increases in α-SMA and collagen I expression in HSCs [27]. Our research also showed that miR-29b suppressed IGFBPrP1-induced HSC autophagy and activation. Atg9a mediates membrane transport to generate autophagosomes during autophagy [28], and it has been reported that formation of LC3 dots is dramatically decreased in Atg9a-knockout MEFs under nutrient-starved condition [28], indicating that Atg9a deficiencies affect autophagy. Similarly, in our study, siAtg9a reduced IGFBPrP1-induced HSC autophagy and activation. IGFBPrP1 thus stimulates HSC autophagy and activation via promoting expression of NEAT1 and Atg9a while suppressing miR-29b.

miR-29a directly targets the 3′UTR region of Atg9a mRNA in ulcerative colitis, suggesting that the miR-29 family is associated with Atg9 [26]. In our study, miR-29b directly regulated Atg9a during IGFBPrP1-induced HSC autophagy and activation, providing more evidences for the direct target of miR-29 family participating in autophagy.

The competitive endogenous RNA (ceRNA) hypothesis states that lncRNAs can cause upregulation of target gene expression by competing for microRNA binding sites. The hypothesis also posits that lncRNAs

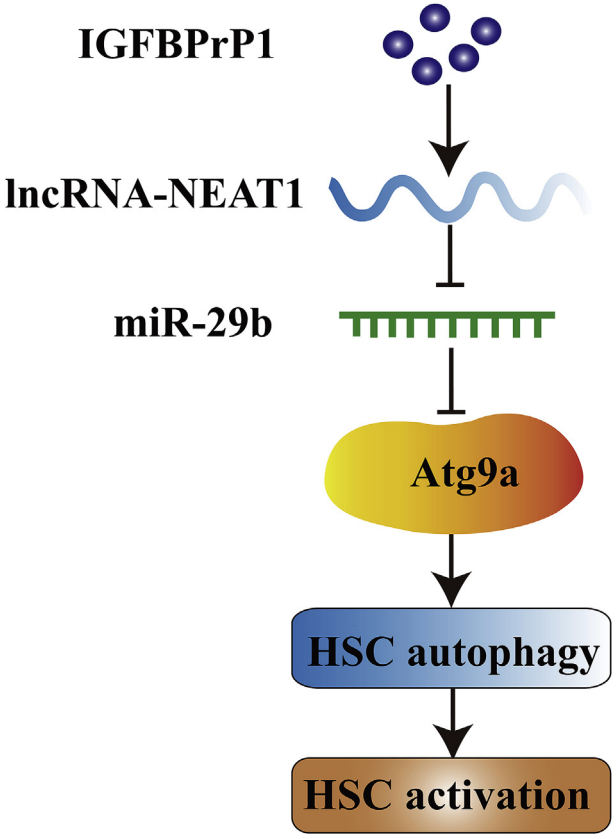

Fig. 6. A schematic illustration explaining the proposed mechanism by which IGFBPrP1 stimulates HSC autophagy and activation through regulation of the NEAT1/miR-29b/Atg9a axis. IGFBPrP1 promotes NEAT1 expression and NEAT1 inhibits miR-29b, thereby upregulating Atg9a, which contributes to HSC autophagy and activation.

can sequestrate miRNA activity, thereby upregulating miRNA target gene expression [29]. miRNA sponges are the antisense RNA transcripts that can inhibit miRNA activity and endogenous miRNA sponges are equivalent to ceRNAs [30]. Several studies have revealed that NEAT1 may act as a ceRNA to sponge miRNA in many diseases. For example, NEAT1 accelerates the progression of liver fibrosis via regulation of microRNA-122 [15] and is involved in sorafenib resistance of hepatocellular carcinoma cells through regulation of miR-335 expression [31]. However, whether NEAT1 is related to miR-29b in IGFBPrP1-induced HSC autophagy and activation was previously unknown. In our study, NEAT1 directly regulated miR-29b to participate in IGFBPrP1-induced HSC autophagy and activation and regulated Atg9a, although direct binding between NEAT1 and Atg9a was not observed. NEAT1 may therefore indirectly regulate Atg9a via direct binding to miR-29b.

Taken together, our study demonstrates the existence of a new NEAT1/miR-29b/Atg9a axis that regulates IGFBPrP1-induced autophagy and activation in HSCs. The mechanism of the NEAT1/miR-29b/Atg9a axis may be explained by the ceRNA hypothesis, as NEAT1 may upregulate Atg9a by sponging miR-29b. However, NEAT1 appears to localize specifically to nuclear paraspeckles [32], which does not support the existence of regulatory interactions between NEAT1 and miR-29b in the cytoplasm [22]. In contrast, NEAT1 release from storage depot paraspeckles and subsequent translocation to the cytoplasm has also been reported [33]. In our study, NEAT1 was found in the cytoplasm of AdIGFBPrP1-treated JS1 cells, therefore it is possible that NEAT1 acts as a ceRNA to regulate miR-29b levels during IGFBPrP1-induced HSC activation.

There are several possible mechanisms by which IGFBPrP1 regulates the NEAT1/miR-29b/Atg9a axis. First, TGFβ1 is related to NEAT1 and can affect miR-29b [15,27]. Mutual regulation of IGFBPrP1 and TGFβ1 has previously been shown, which likely promotes HSC activation [4]. It is possible that IGFBPrP1 directly regulates the NEAT1/miR-29b/Atg9a axis, which needs to be validated in future studies. Secondly, NEAT1 is also a known p53 target gene [34], and nuclear factor-kappa B (NF-κB) is able to bind to the NEAT1 promoter region [35]. In addition, out previous study has shown that IGFBPrP1 is related to the NF-κB or p53 pathway [6], therefore, it is possible that IGFBPrP1 regulates NF-κB or p53, which bind NEAT1 to further modulate the NEAT1/miR-29b/Atg9a axis.

This study showed that IGFBPrP1 increased NEAT1, Atg9a and autophagy, but suppressed miR-29b levels in mouse liver tissue. However, the effects of NEAT1, miR-29b, and Atg9a on IGFBPrP1-induced HSC autophagy and activation were only explored *in vitro,* which is the limitation of this study, thus further investigation is needed to elucidate the effects of NEAT1, miR-29b and Atg9a on HSC autophagy and activation during IGFBPrP1-induced mouse liver fibrosis *in vivo*.

5. Conclusion

This study demonstrated that NEAT1, Atg9a, and autophagy are upregulated while miR-29b is downregulated by IGFBPrP1 *in vivo* and *in vitro*. In addition, IGFBPrP1-induced HSC autophagy and activation is stimulated by NEAT1 and inhibited by miR-29b, and Atg9a participates in IGFBPrP1-induced HSC autophagy and activation. Importantly, NEAT1, miR-29b, and Atg9a form a NEAT1/miR-29b/Atg9a axis to regulate IGFBPrP1-induced HSC autophagy and activation (Fig. 6). Our study thus elucidates a novel mechanism of IGFBPrP1-induced HSC activation and may provide new insights into the pathogenesis and treatment of liver fibrosis.

Declaration of competing interest

The authors declare no conflicts of interest.

Acknowledgement

This study was supported by grants from National Natural Science Foundation of China (81670559); sponsored by the Fund for Shanxi Key Subjects Construction (FSKSC), sponsored by the Fund for Shanxi “1331 Project” Key Subjects Construction (1331KSC); Shanxi Medical University Key Laboratory of Cellular Physiology, Ministry of Education; Key Research and Development Project of Shanxi Province (201603D421023).

Appendix A. Supplementary data

Supplementary data to this article can be found online at https://doi.org/10.1016/j.lfs.2019.116902.

References

[1] L. Campana, J.P. Iredale, Regression of liver fibrosis, Semin. Liver Dis. 37 (2017) 1–10.
[2] R. Harris, D.J. Harman, T.R. Card, G.P. Aithal, I.N. Guha, Prevalence of clinically significant liver disease within the general population, as defined by non-invasive markers of liver fibrosis: a systematic review, Lancet Gastroenterol. Hepatol. 2 (2017) 288–297.
[3] T. Higashi, S.L. Friedman, Y. Hoshida, Hepatic stellate cells as key target in liver fibrosis, Adv. Drug Deliv. Rev. 121 (2017) 27–42.
[4] X.-Q. Li, Q.-Q. Zhang, H.-Y. Zhang, X.-H. Guo, H.-Q. Fan, L.-X. Liu, Interaction between insulin-like growth factor binding protein-related protein 1 and transforming growth factor beta 1 in primary hepatic stellate cells, Hepatobiliary Pancreat. Dis. Int. 16 (2017) 395–404.
[5] Y. Guo, Y. Zhang, Q. Zhang, X. Guo, H. Zhang, G. Zheng, L. Liu, Insulin-like growth factor binding protein-related protein 1 (IGFBPrP1) contributes to liver inflammation and fibrosis via activation of the ERK1/2 pathway, Hepatol Int 9 (2015) 130–141.
[6] X. Guo, H. Zhang, Q. Zhang, X. Li, L. Liu, Screening for and validation of a hepatic fibrosis-related pathway induced by insulin-like growth factor-binding protein-

related protein 1, Eur. J. Gastroenterol. Hepatol. 28 (2016) 762–772.
[7] V. Hernandez-Gea, Z. Ghiassi-Nejad, R. Rozenfeld, R. Gordon, M.I. Fiel, Z. Yue, M.J. Czaja, S.L. Friedman, Autophagy releases lipid that promotes fibrogenesis by activated hepatic stellate cells in mice and in human tissues, Gastroenterology 142 (2012) 938–946.
[8] Z. Zhang, R. Singh, M. Aschner, Methods for the detection of autophagy in mammalian cells, Curr Protoc Toxicol 69 (2016) 20.12.21-20.12.26.
[9] Y. Feng, D.J. Klionsky, Autophagic membrane delivery through ATG9, Cell Res. 27 (2017) 161–162.
[10] J.L. Webber, S.A. Tooze, New insights into the function of Atg9, FEBS (Fed. Eur. Biochem. Soc.) Lett. 584 (2010) 1319–1326.
[11] Y. He, S. Hwang, Y. Cai, S.J. Kim, M. Xu, D. Yang, A. Guillot, D. Feng, W. Seo, X. Hou, B. Gao, MicroRNA-223 ameliorates nonalcoholic steatohepatitis and cancer by targeting multiple inflammatory and oncogenic genes in hepatocytes, Hepatology (2019), https://doi.org/10.1002/hep.30645.
[12] C. Roderburg, G.W. Urban, K. Bettermann, M. Vucur, H. Zimmermann, S. Schmidt, J. Janssen, C. Koppe, P. Knolle, M. Castoldi, F. Tacke, C. Trautwein, T. Luedde, Micro-RNA profiling reveals a role for miR-29 in human and murine liver fibrosis, Hepatology 53 (2011) 209–218.
[13] J. Zhu, Z. Luo, Y. Pan, W. Zheng, W. Li, Z. Zhang, P. Xiong, D. Xu, M. Du, B. Wang, J. Yu, J. Zhang, J. Liu, H19/miR-148a/USP4 axis facilitates liver fibrosis by enhancing TGF-beta signaling in both hepatic stellate cells and hepatocytes, J. Cell. Physiol. 234 (2019) 9698–9710.
[14] Q.M. Wang, G.Y. Lian, Y. Song, Y.F. Huang, Y. Gong, LncRNA MALAT1 promotes tumorigenesis and immune escape of diffuse large B cell lymphoma by sponging miR-195, Life Sci. (2019), https://doi.org/10.1016/j.lfs.2019.03.040.
[15] F. Yu, Z. Jiang, B. Chen, P. Dong, J. Zheng, NEAT1 accelerates the progression of liver fibrosis via regulation of microRNA-122 and Kruppel-like factor 6, J. Mol. Med. (Berl.) 95 (2017) 1191–1202.
[16] P.G. Thomes, E. Brandon-Warner, T. Li, T.M. Donohue Jr., L.W. Schrum, Data on the effect of pro-fibrotic cytokine TGF-beta on hepatic stellate cell autophagy, Data Brief 10 (2017) 312–314.
[17] W. Chen, Z. Zhang, Z. Yao, L. Wang, F. Zhang, J. Shao, A. Chen, S. Zheng, Activation of autophagy is required for Oroxylin A to alleviate carbon tetrachloride-induced liver fibrosis and hepatic stellate cell activation, Int. Immunopharmacol. 56 (2018) 148–155.
[18] T.J. Huang, J.J. Ren, Q.Q. Zhang, Y.Y. Kong, H.Y. Zhang, X.H. Guo, H.Q. Fan, L.X. Liu, IGFBPrP1 accelerates autophagy and activation of hepatic stellate cells via mutual regulation between H19 and PI3K/AKT/mTOR pathway, Biomed. Pharmacother. 116 (2019) 109034.
[19] J. Chen, Y. Yu, S. Li, Y. Liu, S. Zhou, S. Cao, J. Yin, G. Li, MicroRNA-30a ameliorates hepatic fibrosis by inhibiting Beclin1-mediated autophagy, J. Cell Mol. Med. 21 (2017) 3679–3692.
[20] K. Zhang, X. Han, Z. Zhang, L. Zheng, Z. Hu, Q. Yao, H. Cui, G. Shu, M. Si, C. Li, Z. Shi, T. Chen, Y. Han, Y. Chang, Z. Yao, T. Han, W. Hong, The liver-enriched lnc-LFAR1 promotes liver fibrosis by activating TGFbeta and Notch pathways, Nat. Commun. 8 (2017) 144.
[21] X.Y. Liu, Y.J. He, Q.H. Yang, W. Huang, Z.H. Liu, G.R. Ye, S.H. Tang, J.C. Shu, Induction of autophagy and apoptosis by miR-148a through the sonic hedgehog signaling pathway in hepatic stellate cells, Am J Cancer Res 5 (2015) 2569–2589.
[22] F. Yu, B. Chen, P. Dong, J. Zheng, HOTAIR epigenetically modulates PTEN expression via MicroRNA-29b: a novel mechanism in regulation of liver fibrosis, Mol. Ther. 25 (2017) 205–217.
[23] J. Li, B. Cen, S. Chen, Y. He, MicroRNA-29b inhibits TGF-beta1-induced fibrosis via regulation of the TGF-beta1/Smad pathway in primary human endometrial stromal cells, Mol. Med. Rep. 13 (2016) 4229–4237.
[24] M. Ma, J. Hui, Q.Y. Zhang, Y. Zhu, Y. He, X.J. Liu, Long non-coding RNA nuclear-enriched abundant transcript 1 inhibition blunts myocardial ischemia reperfusion injury via autophagic flux arrest and apoptosis in streptozotocin-induced diabetic rats, Atherosclerosis 277 (2018) 113–122.
[25] W. Yan, Z.Y. Chen, J.Q. Chen, H.M. Chen, LncRNA NEAT1 promotes autophagy in MPTP-induced Parkinson's disease through stabilizing PINK1 protein, Biochem. Biophys. Res. Commun. 496 (2018) 1019–1024.
[26] Y. Xu, J. Yang, F. Li, G. Lian, M. Ouyang, MiR-29a inhibited intestinal epithelial cells autophagy partly by decreasing ATG9A in ulcerative colitis, Anti Canccer Drugs 29 (2018) 652–659.
[27] C. Liang, S. Bu, X. Fan, Suppressive effect of microRNA-29b on hepatic stellate cell activation and its crosstalk with TGF-beta1/Smad3, Cell Biochem. Funct. 34 (2016) 326–333.
[28] T. Saitoh, N. Fujita, T. Hayashi, K. Takahara, T. Satoh, H. Lee, K. Matsunaga, S. Kageyama, H. Omori, T. Noda, N. Yamamoto, T. Kawai, K. Ishii, O. Takeuchi, T. Yoshimori, S. Akira, Atg9a controls dsDNA-driven dynamic translocation of STING and the innate immune response, Proc. Natl. Acad. Sci. U. S. A. 106 (2009) 20842–20846.
[29] L. Salmena, L. Poliseno, Y. Tay, L. Kats, P.P. Pandolfi, A ceRNA hypothesis: the Rosetta Stone of a hidden RNA language? Cell 146 (2011) 353–358.
[30] D.W. Thomson, M.E. Dinger, Endogenous microRNA sponges: evidence and controversy, Nat. Rev. Genet. 17 (2016) 272–283.
[31] S. Chen, X. Xia, Long noncoding RNA NEAT1 suppresses sorafenib sensitivity of hepatocellular carcinoma cells via regulating miR-335-c-Met, J. Cell. Physiol. (2019), https://doi.org/10.1002/jcp.27567.
[32] X. Yu, Z. Li, H. Zheng, M.T. Chan, W.K. Wu, NEAT1: a novel cancer-related long non-coding RNA, Cell Prolif 50 (2017).
[33] P. Zhang, L. Cao, R. Zhou, X. Yang, M. Wu, The lncRNA Neat1 promotes activation of inflammasomes in macrophages, Nat. Commun. 10 (2019) 1495.
[34] S.S. Mello, C. Sinow, N. Raj, P.K. Mazur, K. Bieging-Rolett, D.K. Broz, J.F.C. Imam, H. Vogel, L.D. Wood, J. Sage, T. Hirose, S. Nakagawa, J. Rinn, L.D. Attardi, Neat1 is a p53-inducible lincRNA essential for transformation suppression, Genes Dev. 31 (2017) 1095–1108.
[35] W. Zhou, X. Chen, Q. Hu, X. Chen, Y. Chen, L. Huang, Galectin-3 activates TLR4/NF-kappaB signaling to promote lung adenocarcinoma cell proliferation through activating lncRNA-NEAT1 expression, BMC Canc. 18 (2018) 580.